Available online at www.sciencedirect.com

jmr&t Journal of Materials Research and Technology

www.jmrt.com.br

Original article

On the pitting resistance of friction stir welded UNS S82441 lean duplex stainless steel

Antonio Marcos dos Santos Leite [a], Maysa Terada [b,c,*], Victor Ferrinho Pereira [c], Eduardo Bertoni da Fonseca [d], Nelson Batista de Lima [a], Isolda Costa [a]

[a] Institute of Energy and Nuclear Researches (IPEN), Center for Materials Science and Technology (CCTM), Av. Prof. Lineu Prestes, 2.242, São Paulo, SP, Brazil

[b] University of São Paulo, EPUSP, Av. Prof. Mello de Moraes, 2463 São Paulo, SP, Brazil

[c] Brazilian Nanotechnology National Laboratory (LNNano), Brazilian Center for Research in Energy and Materials (CNPEM), Rua Giuseppe Maximo Scolfaro, 10,000 Campinas, SP, Brazil

[d] School of Mechanical Engineering, University of Campinas, Rua Mendeleyev, 200, Cidade Universitária "Zeferino Vaz", Campinas, SP, Brazil

ARTICLE INFO

Article history:
Received 7 August 2018
Accepted 8 May 2019
Available online 1 June 2019

Keywords:
Electrochemical tests
Electron microscopy
Duplex stainless steel
FSW

ABSTRACT

Friction stir welding has been considered as an alternative to fusion welding processes of stainless steels. A lean duplex stainless steel, grade UNS S82441, has been recently developed and is prone to localized corrosion, such as pitting when exposed to harsh conditions during use. However, pitting resistance of UNS S82441 has not been previously investigated. In this study, UNS S82441 lean duplex stainless steel was friction stir welded, and its microstructure and localized corrosion resistance were investigated by phase volumetric fraction, scanning electron microscopy, transmission electron microscopy and electrochemical tests. The pitting resistance of each zone was investigated by polarization tests and by determining the critical pitting temperature. The results indicated that microstructural changes promoted by friction stir welding affected the pitting resistance of the lean duplex stainless steel.

1. Introduction

Duplex stainless steels have been widely used in the manufacture of equipment and piping of different segments, such as chemical, nuclear, pulp & paper, and oil & gas. The major limitation of these stainless steels is the precipitation of deleterious phases whenever they are exposed to high temperatures; such is the case in conventional fusion welding processes. This severely reduces the corrosion resistance and mechanical properties of these materials [1–4]. However, in friction stir welding (FSW), precipitation is avoided due to the brief period of exposure at elevated temperatures followed by rapid cooling. FSW is a solid-state joining technique in which materials are heated and stirred by a non-consumable tool. This process is based on the plastic deformation of materials without reaching their melting points. Thus, many of the problems associated with fusion welding techniques are

* Corresponding author.
E-mail: maysaterada@uol.com.br (M. Terada).

https://doi.org/10.1016/j.jmrt.2019.05.010

prevented by FSW, resulting in welded joints of superior properties compared to those obtained by conventional processes [5].

The effect of conventional fusion welding processes on the corrosion resistance of duplex stainless steels has been much investigated [6–10]. In general, the heat affected zone (HAZ) presents lower corrosion resistance than the unaffected base metal, due to the modification in the ferrite/austenite ratio caused by precipitation of deleterious phases and partitioning of alloying elements. Tan et al. [11] and Chen et al. [12] investigated the influence of plasma arc welding (PAW) on the corrosion resistance of UNS S32304 steel and studied the relationship between the distribution of Cr, Mo, Ni, and N alloying elements in ferrite (α) and austenite (γ) and the corrosion resistance of these phases in the different zones resulting from PAW. The literature [11,12] also reports estimates of Cr, Ni and Mo contents in ferrite and austenite in each welding zone. Increased concentration of Cr and Mo was observed in ferrite, while an increase in Ni was detected in austenite. Such differences were more significant in the HAZ.

The partitioning of alloying elements between austenite and ferrite alters their pitting resistance equivalent number (PREN), which is an empirical number given by Eq. (1) used to rank grades of duplex stainless steels [13,14]. Usually, a decrease in the PREN of ferrite is observed in the HAZ, which suggests it is more susceptible to localized corrosion than austenite.

$$\mathrm{PREN} = \%\,\mathrm{Cr} + 3.3 \times \%\,\mathrm{Mo} + 16 \times \%\,\mathrm{N} \quad (1)$$

In duplex stainless steels, the main alloying elements, such as Cr, Ni, Mo and N, are not homogeneously distributed in austenite and ferrite. Cr and Mo are preferentially found in ferrite, while N and Ni are found in austenite. Consequently, the PREN of each phase might vary, as well as their pitting corrosion resistance. According to the literature [15,16], the pitting corrosion resistance of duplex stainless steels is dominated by the PREN of the most susceptible phase.

Published works [5,17,18] report good mechanical properties associated with FSW of duplex stainless steels. However, concerning the corrosion resistance of FSWed duplex stainless steels, there are still few studies [19,20]. Magnani et al. [19] investigated the corrosion resistance of two duplex stainless steel sheets, UNS S32205 and UNS S32101, and found good properties associated with these welded steels. Park et al. evaluated the corrosion resistance of the advancing side of the stir zone and the heat affected zone (HAZ) of the FSWed AISI 304 stainless steel [21]. Garcia et al. studied the pitting corrosion of four different zones of welded austenitic stainless steels (AISI 304 and 316L). The results showed that the HAZ was the most critical zone for pitting corrosion for both materials due to sensitization [22]. However, no work was found on the corrosion resistance of the alloy used in this study, UNS S82441, a recently-developed lean duplex stainless steel with high nitrogen content (0.234 wt.%), which was incorporated to ASTM specifications in 2011 [23]. The nitrogen content of this alloy is superior to that of the UNS S32205, which is the most used duplex stainless steel. Consequently, the results of this study are new and they reflect the effect of nitrogen on the corrosion resistance of this grade.

UNS S82441 lean duplex stainless steel has an excellent combination of mechanical properties and corrosion resistance, which makes them technically and economically superior to other grades of stainless steels, such as AISI 304L (UNS S30403) and 316L (UNS S31603) austenitic stainless steels, and 2101 (UNS S32101) or 2304 (UNS S32304) duplex stainless steels [24]. In UNS S82441, Ni is partially replaced by other austenite-stabilizer elements, such as Mn and N, while its Mo content is lower than that of other duplex steels. The amount of alloying elements in UNS S82441 is smaller compared to the conventional duplex stainless steels (UNS S31803/UNS S32205) [24]. Zhao et al. [25] investigated the effect of ageing time at 700 °C on the intergranular corrosion resistance of the UNS S82441 steel by electrochemical methods. They also carried out microstructural characterization by scanning electron microscopy (SEM) and transmission electron microscopy (TEM) and found out that Cr_2N and $M_{23}C_6$, sigma and chi phases nucleated simultaneously at the initial stages of ageing. When ageing time was extended to 48 h, sigma phase grew larger, and intergranular corrosion became more severe and progressed from intergranular to uniform corrosion.

Nevertheless, this steel is still an object of investigation, and the effect of FSW on its corrosion resistance needs further studies [20]. The literature on the impact of FSW on pitting resistance of duplex stainless steel is scarce and even rarer for lean duplex stainless steels. This present study aims to assess the effect of FSW on the microstructure and localized corrosion resistance of the UNS S82441 lean duplex stainless steel in the various zones resulting from friction stir welding.

2. Methods

Cold-rolled and solubilized UNS S82441 lean duplex stainless steel sheets with dimensions of 350 mm (length) × 70 mm (width) × 8.0 mm (thickness) were provided for this study. The chemical composition was obtained using optical emission spectroscopy, and the results are shown in Table 1, along with the nominal composition. It can be seen that all alloying elements are within the nominal range according to specifications [26].

The sheets were joined by friction stir welding (FSW) at LNNano/CNPEM facilities using a Manufacturing Technology Inc. machine, model RM1. The temperature was measured near the non-consumable pin, and the maximum temperature reached in the process was below 720 °C. The non-consumable tool consisted of a 25 mm shoulder diameter and a 5.7 mm long conical pin of polycrystalline cubic boron nitride (PCBN) composed of 40 vol.% of W and 25 at.% Re. The rotational speed used was 200 rpm, the welding speed of the tool was 100 mm/min, and the axial force was 40–50 kN. All welds were produced in position control mode.

The FSWed plate was etched to identify the different zones, then small samples were taken from the top surface of each zone. The microstructure of the zones after FSW was revealed by electrolytic etching in 40% NaOH solution. A voltage of 1.5 V was applied for 60 s to expose the grain boundaries and the ferrite/austenite interface, according to ASTM A923 [27].

Table 1 – Chemical composition (wt.%) of UNS S82441 lean duplex stainless steel [16].

Chemical composition	Elements (wt.%)										
	C	Si	Mn	P	S	Cr	Ni	Mo	N	Cu	Fe
Nominal	0.030 (max.)	0.7 (max.)	2.5–4.0	0.035 (max.)	0.005 (max.)	23.0–25.0	3.0–4.5	1.0–2.0	0.20–0.30	0.10–0.80	Balance
Analyzed	0.020	0.341	2.705	0.019	0.002	24.034	3.459	1.550	0.234	0.305	

The specimens analyzed using electrochemical tests were mounted in bakelite, leaving an area of 0.3 cm^2 for exposure to the electrolyte. The relatively small area exposed to the electrolyte was due to the width of the TMAZ. Consequently, the same exposure area was used for all the tested zones. Surface preparation of the working electrodes was carried out by grinding with SiC paper followed by polishing with diamond paste to a 1 μm surface finish.

Microstructural characterization was carried out by Optical Microscopy (OM) (Olympus, Model GX51), Scanning Electron Microscopy (SEM) (Leica, Stereoscan 440), EDS analysis (Oxford, Model Inca X-ACT) and Transmission Electron Microscopy (TEM) (Phillips Model CM200 SuperTwin). A detector coupled to the SEM was used to perform a semiquantitative analysis of ferrite (α) and austenite (γ) by X-ray energy dispersive spectroscopy (EDS), with the aim of estimating the PREN of each phase. The depth of penetration of EDS was 3 μm. Fe, Cr, Ni, Mo, Mn, Si, and Cu were analyzed by the EDS. N could not be quantified by this technique due to the limitation of the EDS analysis for elements with $Z < 11$ [28]. In the literature [15,23,29], this is circumvented by assuming N saturation in ferrite (nearly 0.05%). The remaining N content in the alloy was ascribed to austenite, according to the calculated phase fraction of each zone. These assumptions are required for estimating the PREN of each phase.

Electrochemical methods were used for characterization of pitting susceptibility. The polarization tests were performed in 0.6 M NaCl solution at (25 ± 2) °C. The tests were initiated after 300 s of immersion in the solution. The sweep in the forward direction was carried out from −0.5 V (SCE) up to 1.4 V (SCE), where the scan direction was reversed, and it was terminated at −0.5 V (SCE). The tests were carried out with a scan rate of 1 mV/s. The localized corrosion resistance in chloride-containing media was investigated by cyclic potentiodynamic polarization tests and by determining the critical pitting temperature (CPT). An electrochemical cell composed of three electrodes was used in both tests. A platinum wire and a saturated calomel electrode (SCE) were used as the counter and reference electrodes, respectively. A potentiostat Autolab (PGSTAT302N) controlled by NOVA software was used in the electrochemical tests.

The critical pitting temperature (CPT) was evaluated by applying a fixed potential of 0.7 V (SCE), corresponding to anodic polarization, on the working electrode immersed in 1 M NaCl solution. To normalize the surface conditions of the different specimens for CPT measurements, a potential of −0.6 V (SCE) was applied for 300 s, before the polarization at 0.7 V. Afterwards, OM and SEM were used to observe the sample surface. A thermostatic bath controlled the temperature increase rate at 1 °C/min, and the current density was continuously recorded. The test was terminated 60 s after the current density reached 100 μA/cm^2. The corresponding temperature is the critical pitting temperature. This method has been used to classify materials according to their pitting corrosion resistance [30,31]. This potentiostatic method for the determination of critical pitting temperature (CPT) was adapted from ASTM G150 [30] and has an accuracy of ±2 °C [31]. The only difference between the method adopted in this study and the ASTM G150 is that there was no N_2 bubbling as indicated by ASTM. According to ARNVIG and BISGARD [32], bubbling is not essential for this test. For all zones evaluated, at least three experiments were carried out to check the reproducibility of the results.

3. Results

In the FSWed plate, four zones were identified, as shown in Fig. 1, according to the different microstructures resultant of different thermal or thermomechanical conditions. FSW is asymmetrical with respect to the centerline of the joint due to the different relative velocities at both sides of the tool. The side in which the tool tangential and translational velocities are on the same direction is called the advancing side (AS), while the side where the tool tangential and translational velocities are opposite (with slower relative speed) is called the retreating side (RS) [33]. The investigated zones were: (1) base metal (BM); (2) thermomechanically affected zone (TMAZ) and its surroundings at the retreating side (RS); (3) stir zone (SZ); and (4) TMAZ and its surroundings at the advancing side (AS). It should be noted that it was not possible to clearly distinguish the HAZ from the BM. The literature reports that no significant microstructural changes exist on the duplex stainless steels, even at high temperatures [5,17]. Optical micrographs of the four zones taken from the top of the welded joint are also shown in Fig. 1. In these images, austenite is the white phase, and ferrite is the dark one. Intermetallic phases were not observed in the optical micrographs. Microstructural changes due to the FSW were observed in terms of grain morphology and size. A significant reduction in grain size was noticed in the SZ compared to the BM, due to dynamic recrystallisation. In the TMAZ, the effect of deformation is seen in the morphology of the elongated and deformed grains following tool rotation and displacement. A clear interface between the SZ and TMAZ at the advancing side is seen in Fig. 1d. However, in the retreating side, a gradual transition between SZ and TMAZ is observed (Fig. 1c), and the morphology of the grains is highly deformed and irregular.

Fig. 2 shows the volumetric fraction of the phases detected by XRD in the investigated FSW zones. XRD analysis only detected ferrite and austenite in all zones. The presence of deleterious phases, such as sigma, commonly found in

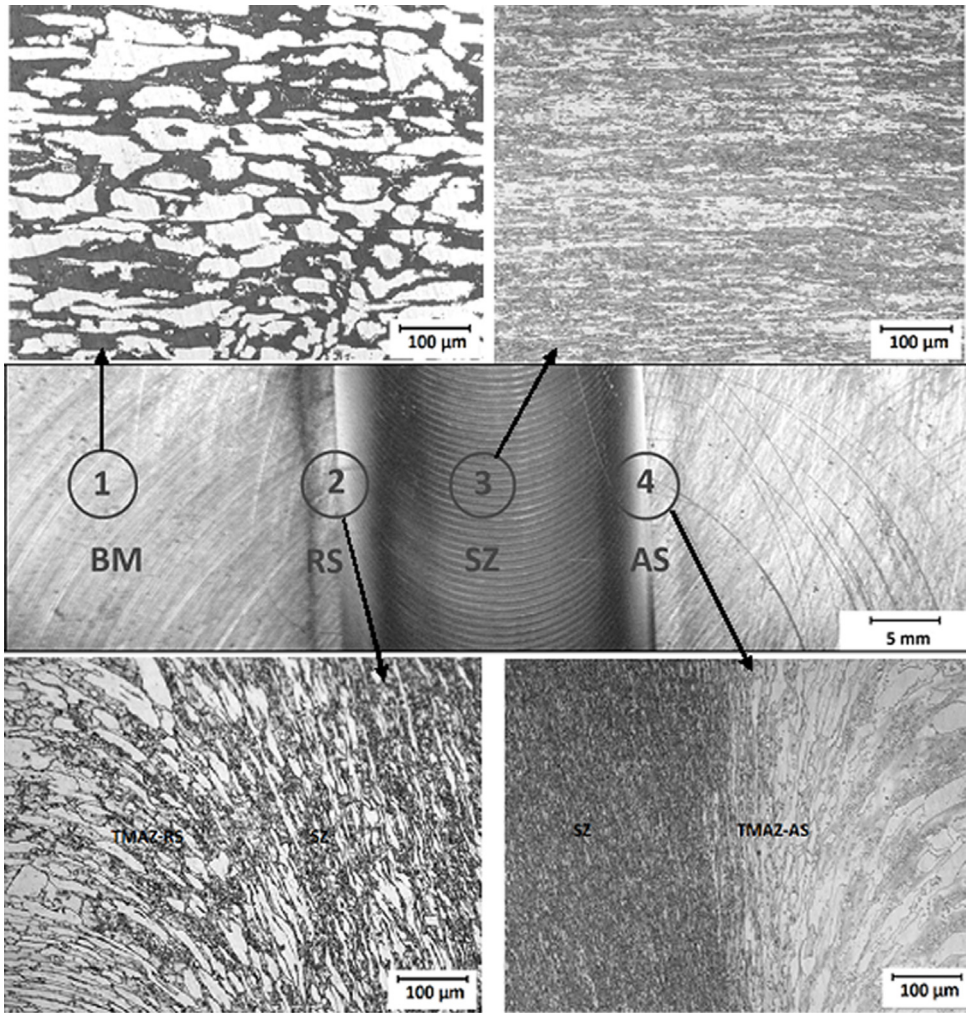

Fig. 1 – Macrograph and optical micrographs of the UNS S82441 steel after Friction Stir Welding. Base metal (BM), thermomechanically affected zone (TMAZ), on retreating side (RS), stir zone (SZ) and thermomechanically affected zone (TMAZ), on advancing side (AS). The ferrite is the white phase and the austenite is the dark one.

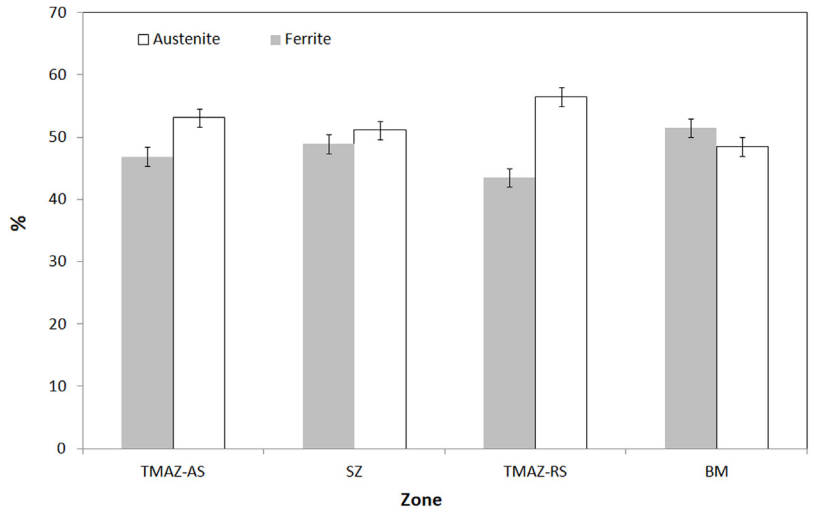

Fig. 2 – Volumetric fraction of the phases detected in the different zones investigated of the steel (*).

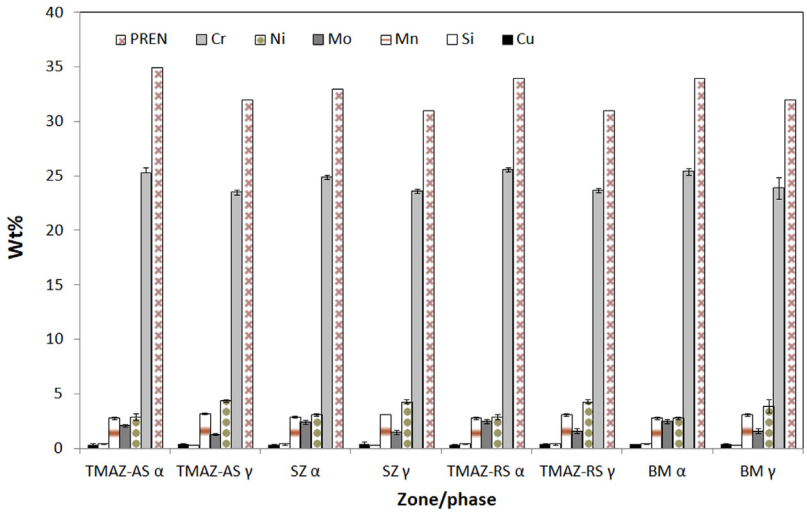

Fig. 3 – Distribution of alloying elements in the ferritic and austenitic phases of the UNS S82441 steel used in this study.

fusion-welded duplex stainless steels, was not identified. If sigma was present at all, it was at a lower volume than the detection limit of 5 vol.% [17]. Also, sigma was not observed in metallography after electrolytic etching with 40% NaOH solution. The results in Fig. 2 also show that ferrite and austenite are found in similar ratios, although the balance tends to shift towards higher austenite volume fraction after FSW.

In order to calculate the PREN of each phase, the alloying elements in ferrite and austenite in each analyzed zone were quantified using X-ray energy dispersive spectroscopy (EDS), except for nitrogen. The results are shown in Fig. 3. Larger amount of Cr and Mo was found in ferrite compared to austenite in the same zone, while Ni was preferentially found in austenite.

Transmission electron microscopy (TEM) of the various zones was also carried out to characterize the effect of FSW on the steel microstructure, and the results are shown in Fig. 4. Fig. 4a shows twins typical of deformation in austenitic grains of the BM indicating that the duplex stainless steel presents residual strain due to the fabrication process, but precipitates were not identified in this zone. In Fig. 4b, dislocations were found inside some grains of the SZ along with dislocation-free zones, indicating partial recovery and recrystallisation. As twins were not found in this zone, it is possible that part of the strain in the BM must have been relieved during FSW. Furthermore, precipitates were not identified in the SZ. More heterogeneous microstructures were associated with the thermomechanically affected zone, which indicates the nucleation of nanometric precipitates at some grain boundaries, and at the advancing side, the development of twins is also indicated.

The corrosion resistance of each zone was analyzed by cyclic polarization tests, and Fig. 5 presents the results obtained. The inset in Fig. 5 shows a schematic polarization curve representative of those obtained in this study, displaying the sweep direction. Passive behaviour is indicated for all the zones tested with current densities of the order of $\mu A/cm^2$ measured in the forward direction of the polarization scan. At potentials of the order of 1.1 V (SCE), the current density increased for all zones, but at current densities of 1 mA/cm^2, the sweep direction was reversed. It was observed that due to the passive film growth during polarization in the forward direction, the corrosion potential at the reverse scan was nobler than that of the forward.

The electrochemical results showed similar polarization curves for the BM and SZ. There were no observable differences in the susceptibility to pitting corrosion and in the hysteresis areas corresponding to these two zones. The main difference between the two zones is the grain size, which is much smaller in the SZ due to intense deformation and recrystallisation, as shown in Fig. 5. However, precipitates were not easily identified, even by TEM micrographs in either of these zones, which explains why they have similar electrochemical behaviour and high resistance to pitting. The retreating and the advancing sides of the reverse scan of the TMAZ have slightly increased passive current densities, indicating a less protective film on these zones during the forward polarization scan. This is related to the highly-deformed grains due to the tool movement leading to heterogeneous microstructures. The heterogeneous microstructure of the TMAZ shown by the TEM micrographs indicates nanometric precipitates inside some grains at the neighbourhood of “clean” grains, with no precipitates inside. Nanometric precipitates are also observed at some grain and subgrain boundaries, which is indicated by the dark areas at these boundaries. This results in the formation of different passive films of lower resistance compared to those formed on the BM and SZ. The increase in current density at potentials of approximately 1.1 V (SCE) could either be due to the localized corrosion or oxygen evolution reaction. Microscopic observation of the surface after polarization tests showed no pitting; this suggests that the increase in current density was related to the oxygen evolution reaction on the alloy surface. Thus, all zones of the FSWed lean duplex stainless steel investigated in this study present high resistance to pitting corrosion. The evaluation of pitting potential at room temperature did not show any noticeable differences

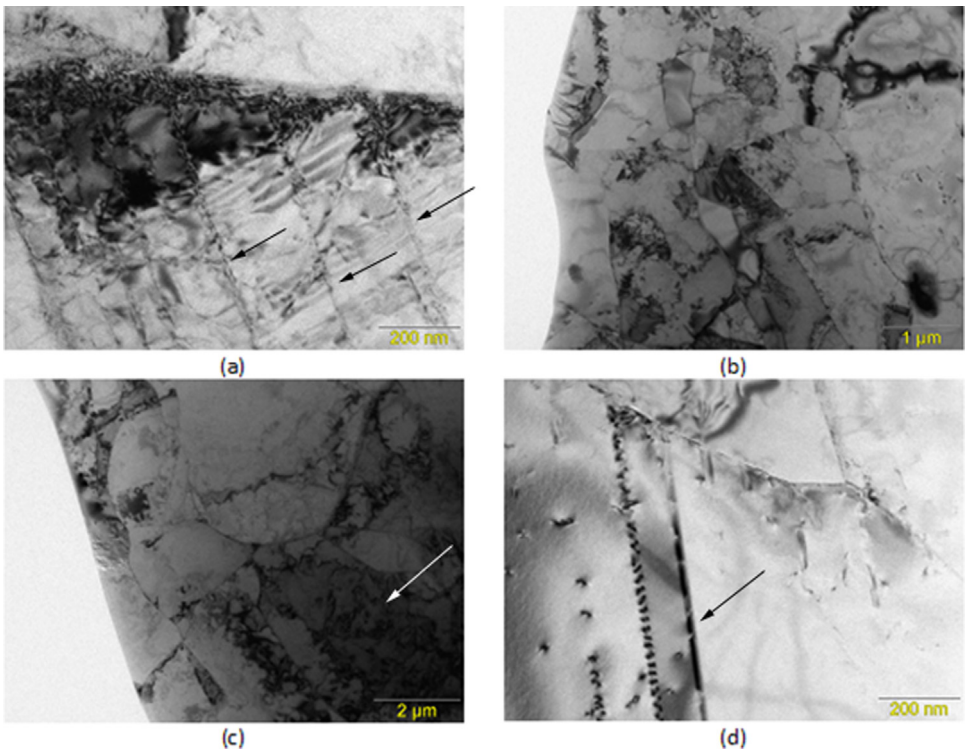

Fig. 4 – Micrographs obtained by transmission electron microscopy (TEM) from: (a) base metal (BM), (b) stir zone (SZ), (c) thermomechanically affected zone-retreating side (TMAZ-RS) and (d) thermomechanically affected zone – advancing side (TMAZ-AS).

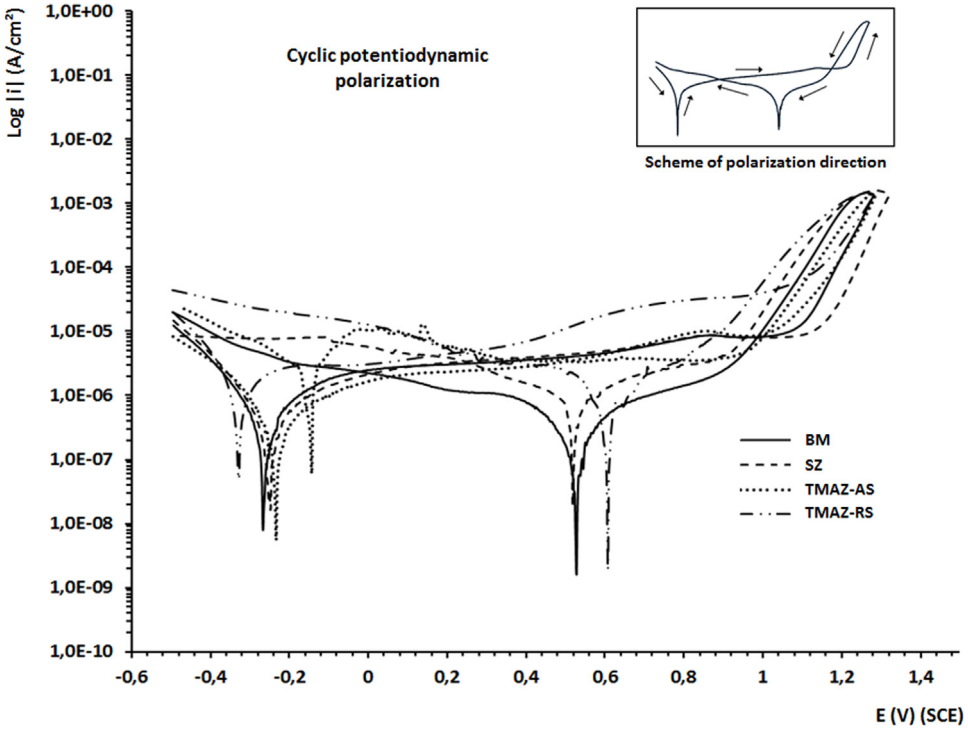

Fig. 5 – Cyclic polarization curves of the four zones of duplex stainless steel UNS S82441 in 0.6 M NaCl solution: BM, SZ, TMAZ-AS, and TMAZ-RS.

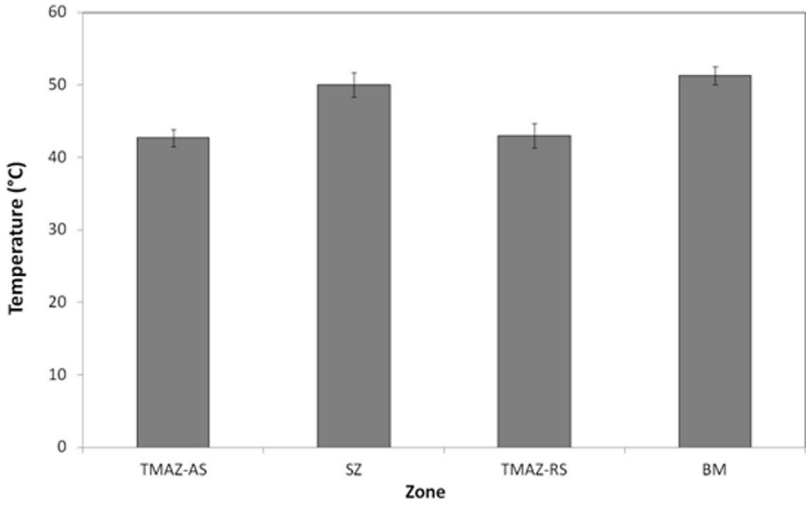

Fig. 6 – Critical pitting temperature of each zone of the UNS S82441 duplex stainless steel (*).

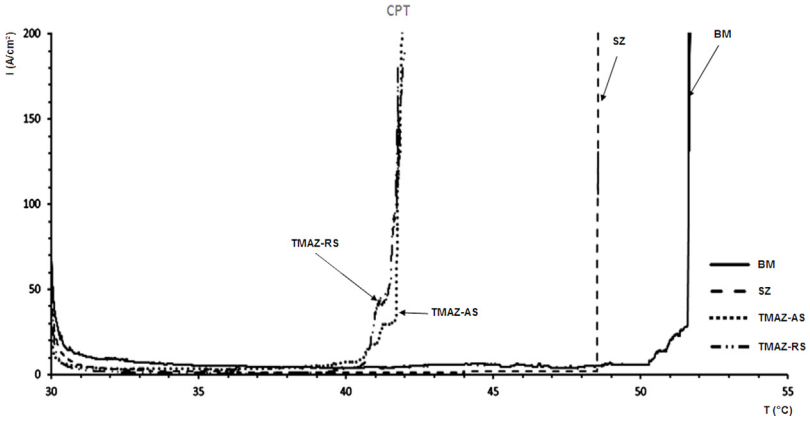

Fig. 7 – Variation of current density with increasing temperature for evaluation of the critical pitting temperatures (CPT) of four zones in the UNS S82441 duplex stainless steel tested in 1.0 M NaCl solution: BM, SZ, TMAZ-AS and TMAZ-RS.

in the localized corrosion resistance of the different zones. Pitting was not detected in the 0.6 M NaCl solution used for the polarization analysis.

As pitting is highly dependent on temperature [31], the critical pitting temperature (CPT) was also evaluated for each zone and the results are shown in Figs. 6 and 7. SEM images of CPT samples to current densities (i) below 10^{-4} A/cm^2 (Fig. 9) revealed that pits nucleated in the ferrite phase. The evolution of corrosion is seen in Fig. 9, with SEM images of CPT samples where current densities were above 10^{-4} A/cm^2.

4. Discussion

According to the literature [14], the best combination of mechanical properties and corrosion resistance of duplex stainless steels is achieved when there is a similar proportion of each phase, that is, approximately 50% ferrite and 50% austenite. High resistance to stress corrosion cracking (SCC), high mechanical strength and toughness are associated with the balance of ferrite and austenite in duplex stainless steels. Fig. 2 shows that TMAZ and SZ present higher austenite contents than the BM. However, comparison of this study with reported literature for fusion welding processes [6–8,24] indicates that FSW maintains an even proportion of both phases, which is not usually found in fusion welding processes. Nonetheless, literature suggests that some ferrite-to-austenite transformation is induced by mechanical work [34], which would lead to N-depleted austenite in the TMAZ zones. This austenite is less resistant to localized (pitting) corrosion, explaining the lower CPT values associated with the TMAZ (Fig. 6).

FSW imposes large deformation at high temperatures due to the thermal energy generated from both, friction and deformation. During this process, thermal gradients are created and might result in microstructural modification, producing different zones, as discussed previously. The α/γ ratio of the UNS S82441 changed in the TMAZ, with a decrease in ferrite volume fraction compared to the base metal. This decrease was lower in the stir zone (SZ). During FSW, an very fast cooling stage that leads to reduced Mo content in the UNS S82441 contributes to the absence of sigma phase [19]. It is worth mentioning that

Mo is one of the main constituents of sigma phase. Also, the studied alloy has considerable amounts of N and Cu, which further decreases the probability of sigma formation [27].

Another point worth mentioning is that FSW practically did not change the distribution of alloying elements in the stir zone (SZ) and in the thermomechanically affected zones (TMAZ) contrary to conventional fusion welding processes.

The results of polarization tests were supported by the evaluation of critical pitting temperature, where the behaviours of the stir zone (SZ) and the base metal (BM) were similar. However, both TMAZ (RS and AS) presented critical pitting temperatures below the BM and SZ. This is explained by the microstructural differences shown in Fig. 4. Precipitates were not found in either, BM or SZ, but the TMAZ showed a more heterogeneous microstructures with the presence of nanometric precipitates. The results of the present study are compatible with literature published elsewhere [4,34,35].

Heyn et al. [36] and Dong et al. [37] proposed a relationship between Cr, Mo and N contents and the critical pitting temperature (CPT) as a theoretical estimate for this last parameter.

$$\mathrm{CPT}(^{\circ}\mathrm{C}) = 2.5 \times \%\,\mathrm{Cr} + 7.6 \times \%\mathrm{Mo} + 31.9 \times \%\,\mathrm{N} - 41 \qquad (2)$$

Based on the duplex stainless steel composition presented in Table 1, the CPT estimated from Eq. [2] for the steel used in this study is 38 °C, which is inferior to the CPT measured in all zones evaluated in this study. A comparison of the estimated CPT with the experimental results shown in Fig. 6 indicates that the various FSW zones present higher pitting corrosion resistance than the predicted. From the CPT results, it was noticed that the TMAZ, both advancing (AS) and retreating sides (RS), were slightly more susceptible to localized corrosion than the BM or SZ, with both sides showing similar pitting susceptibilities. FSW did not significantly change the distribution of the alloying elements but caused grain refinement.

Deng et al. [38], Ebrahimi et al. [39], and Eghbali et al. [40] evaluated the CPT of duplex stainless steels in chloride solutions and found that pitting was always observed preferentially in austenite. Deng et al. [38] found that metastable pits were mainly located near grain boundaries in austenite. However, the authors explained that the lower pitting resistance of austenite was caused by its lower PREN. They also observed that stable pits resulted in the selective corrosion of austenite in the UNS S31803 steel of their investigation. Similar results to those of Deng et al. [38] were also obtained by Eghbali et al. [40], who found that pitting nucleated at the austenite/ferrite interface and propagated towards austenite. They associated this with chromium depletion at the austenite/ferrite interface. In the present study, the PREN estimated for austenite was slightly higher than that of ferrite in all zones, but the nucleation of pitting occurred mainly in the ferrite, as shown in Fig. 8. Ebrahimi et al. [39] also observed that metastable pits formed either in austenite or at the austenite/ferrite interface and associated the higher pitting susceptibility of austenite with its lower PREN compared with ferrite. Surface observation after potentiostatic polarization at 55 °C revealed the presence of propagated stable pits in austenite and at the austenite/ferrite interface. The authors ascribed the location of pitting nucleation in either austenite or at the austenite/ferrite interface, to the lower PREN of the austenite and to the chromium depletion at the austenite/ferrite interface, or to even to the higher density of inclusions at that interface.

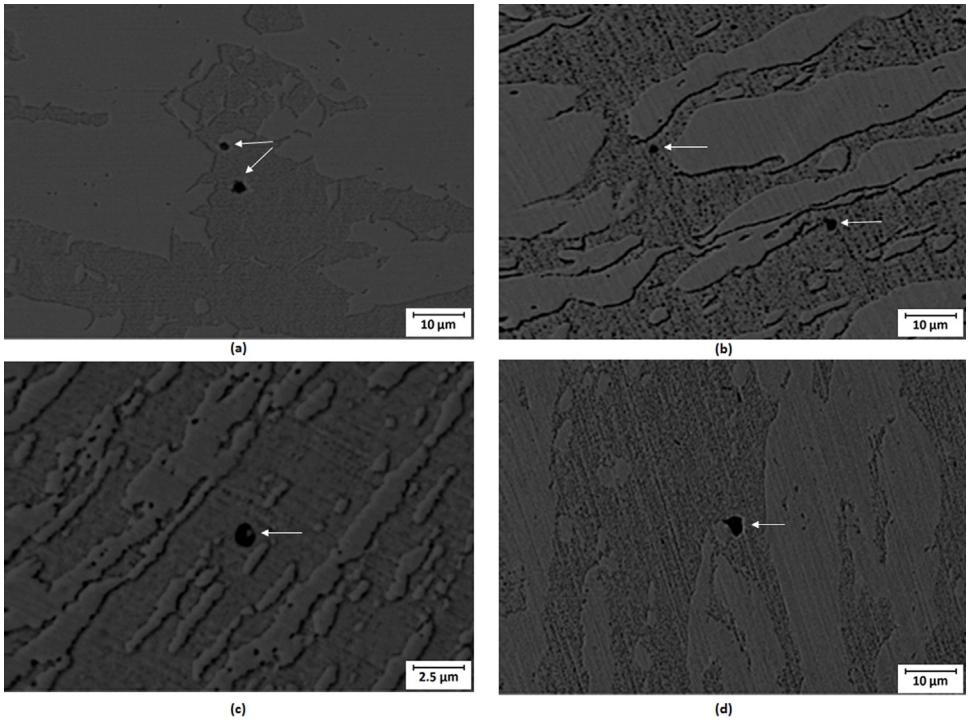

Fig. 8 – Micrographs obtained by SEM after CPT to current density values limited to 10^{-4} A/cm^2 showing: (a) base metal (BM), (b) TMAZ-RS, (c) stir zone (SZ) and (d) TMAZ-AS. Small pits are formed in the ferrite phase or at the ferrite/austenite interface.

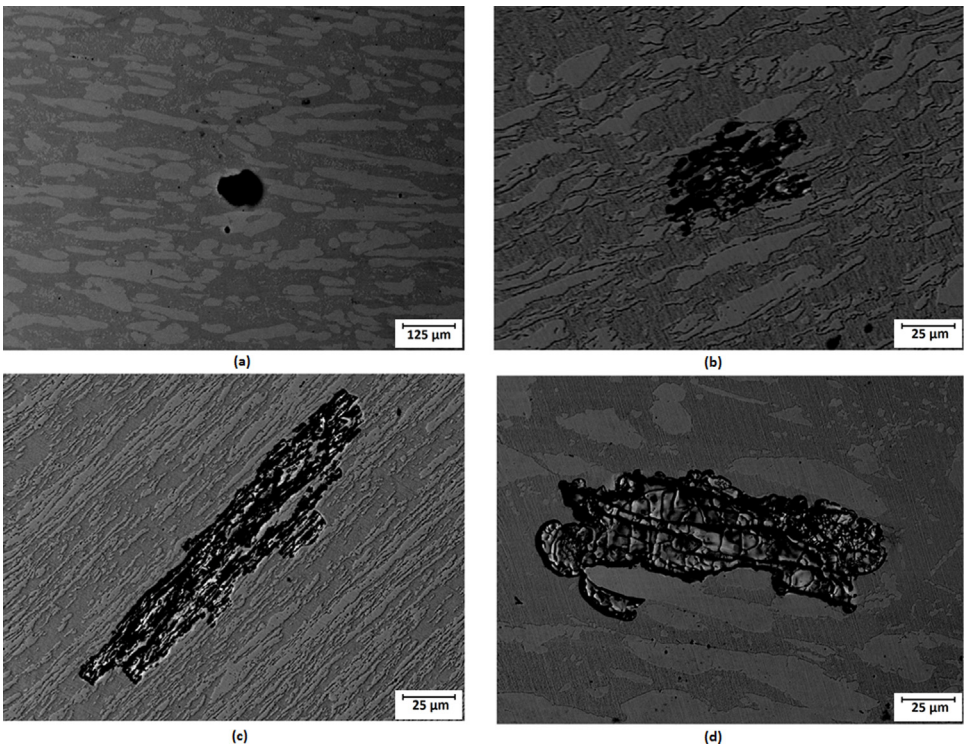

Fig. 9 – Micrographs obtained by SEM after CPT to current density values above 10^{-4} A/cm^2 showing: (a) base metal (BM), (b) region of TMAZ-RS, (c) stir zone (SZ) and (d) region of TMAZ-AS.

The results of this study, contrary to many works in the literature [38–42], showed that pitting nucleated in ferrite or at the ferrite/austenite interface. However, this behaviour is in accordance with the estimated values of PREN for each phase. Nevertheless, PREN must be used with caution for evaluation of pitting susceptibility. It must also be taken into consideration that PREN is based only on chemical composition and it neglects factors such as microstructural characteristics, grain size, deformation of grains, surface finish, temperature, pH of the media, phase balance, and the presence of inclusions and precipitates, which certainly influence the pitting corrosion resistance [29,41]. Besides taking the importance of the chemical composition for pitting corrosion resistance into account, it is worth mentioning that the PREN only considers Cr, Mo and N contents, but disregards the effects of deleterious elements such as P and S, and the partitioning of other important elements in duplex stainless steels, such as Ni [29]. It also disregards the synergistic effect of elements (such as Mn and N [13], Mo and N [15] and Cu and N [15]), which improves the pitting corrosion resistance.

Despite the importance of factors other than the chemical composition, such as the microstructure and deformation state, the influence of some alloying elements in the steel composition is significant, such as the nitrogen content. It is noteworthy that the duplex stainless steel grade used in this study contains a large content of N. Consequently, one of the possible reasons for the higher pitting resistance of the austenite compared to ferrite is the higher N content of the first. Miura et al. [42] investigated the effect of Ni and N contents on the pitting corrosion resistance of the 22% Cr–3% Mo duplex stainless steels welded by Gas Tungsten Arc Welding (GTAW), in which Ni and N contents were varied independently. The critical pitting temperature was evaluated, and the pitting initiation site was observed. The authors found out that the pitting corrosion resistance of austenite was mainly dominant in the base metal. The increase of N in the alloy resulted in increased N content in austenite and improved the corrosion resistance of stainless steel.

Lothongkum et al. [43] studied the effect of N on the corrosion behaviour of 28Cr–7Ni duplex stainless steel with N contents varying from 0 to 0.34% in air-saturated 3.5% NaCl solutions of various pH by potentiodynamic methods. The austenite volume fractions of the tested steels were between 0.35 and 0.64. Corrosion rate decreased with N content at pH 2 and pitting potential increased at all tested pH. They proposed that either N participated in the passive film or it was involved in the reaction to build up a passive film. The metal/passive film interface was enriched with N, which increased the pitting potential. Austenite was preferably corroded in the steel with no N content, whereas ferrite was corroded in steels with higher N content, even though ferrite had higher Cr contents than austenite. Thus, it is believed that the higher amount of nitrogen in the austenite of the UNS S82441 may be the reason for the higher pitting resistance of austenite in the present study. Garfias-Mesias et al. [15] also observed that in chloride containing acidic environments, pitting in duplex stainless steel occurred preferentially in ferrite.

5. Conclusions

- Friction stir welding (FSW) generated different welding zones and affected the corrosion resistance of some of the zones in the UNS S82441 lean duplex stainless steel.
- The TMAZ was the zone most susceptible to pitting with CPT about 10 °C lower than that of the BM or SZl.
- The pitting resistance of the stir zone (SZ) was similar to that of the base metal (BM).
- The austenite phase presented higher resistance to localized corrosion than ferrite. Pitting nucleated in ferrite or at the ferrite/austenite interface.

Conflicts of interest

The authors declare no conflicts of interest.

Acknowledgements

The authors acknowledge CENPES for providing the steel for study, to Brazilian Nanotechnology National Laboratory (LNNano) for FSW, to Rafael Maia from Laboratory of Microstructural Characterization Hubertus Colpaert and Cesar Suzuki from CBC Heavy Industries for the support in the metallographic preparation.

REFERENCES

[1] Linton VM, Laycock NJ, Thomsen SJ, Klumpers A. Failure of a super duplex stainless steel reaction vessel. Eng Failure Anal 2004;11:243–56.
[2] Paulraj P, Garg R. Effect of intermetallic phases on corrosion behaviour and mechanical properties of duplex stainless steel and super-duplex stainless steel. Adv Sci Technol Res J 2015;27:87–105 https://doi.org/10.12913/22998624/59090.
[3] Pohl M, Storz O, Glogowski T. Effect of intermetallic precipitations on the properties of duplex stainless steel. Mater Charact 2007;58:65–71 https://doi.org/10.1016/j.matchar.2006.03.015.
[4] Sieurin H, Sandström R. Sigma phase precipitation in duplex stainless steel 2205. Mater Sci Eng A 2007;444:271–6 https://doi.org/10.1016/j.msea.2006.08.107.
[5] Esmailzadeh M, Shamanian M, Kermanpur A, Saeid T. Microstructure and mechanical properties of friction stir welded lean duplex stainless steel. Mater Sci Eng A 2013;561:486–91 https://doi.org/10.1016/j.msea.2012.10.068.
[6] Alvarez TR, et al. Influence of interpass temperature on the properties of duplex stainless steel during welding by the submerged arc welding process. Soldag Insp 2014;19:114–24 https://doi.org/10.1590/0104-9224/SI1902.03.
[7] Borsato KS. Microstructural and mechanical properties characterization of thick plates of UNS 31803 duplex stainless steel exposed to welding thermal cycles. [PhD thesis]. Florianopolis: Federal University of Santa Catarina; 2001.
[8] Kordatos JD, Fourlaris G, Papadimitriou G. The effect of cooling rate on the mechanical and corrosion properties of SAF 2205 (UNS 31803) duplex stainless steel welds. Scr Mater 2001;44:401–8 https://doi.org/10.1016/S1359-6462(00)00613-8.
[9] Nunes EB, et al. Effect of the welding heat input on the microstructure and mechanical properties of the heat affected zone of multi-pass welded joints of duplex stainless steel. Soldag Insp 2011;16:223–31 https://doi.org/10.1590/S0104-92242011000300004.
[10] Souza CS, et al. Evaluation of multipass welding of thick lean duplex stainless steel UNS S32304 plates welded by SMAW. GMAW and FCAW – Part II – corrosion resistance. Soldag Insp 2013;18:257–67 https://doi.org/10.1590/S0104-92242013000300008.
[11] Tan H, et al. Annealing temperature effect on the pitting corrosion resistance of plasma arc welded joints of duplex stainless steel UNS S32304 in 1.0 M NaCl. Corros Sci 2011;53:2191–200 https://doi.org/10.1016/j.corsci.2011.02.041.
[12] Chen L, Tan H, Wang Z, Li J, Jiang Y. Influence of cooling rate on microstructure evolution and pitting corrosion resistance in the simulated heat-affected zone of 2304 duplex stainless sheets of steel. Corros Sci 2012;58:168–74 https://doi.org/10.1016/j.corsci.2012.01.018;
Thomas WM, Nicholas ED, Needham JC, Murch MG, Temple-Smith P, Dawes CJ. Friction Welding. US Pat. 5.460.317 A. 24 out; 1995. p. 19.
[13] Gunn R. Duplex stainless steels: microstructure, properties and applications. first ed. Cambridge: Abington Publishing; 1997.
[14] Alvarez-Armas I. Duplex stainless steels: a brief history and some recent alloys. Recent Pat Mech Eng 2008:51–7 https://doi.org/10.2174/2212797610801010051.
[15] Garfias-Mesias LF, Sykes JM, Tuck CDS. The effect of phase compositions on the pitting corrosion of 25 Cr duplex stainless steel in chloride solutions. Corros Sci 1996;38:1319–30 https://doi.org/10.1016/0010-938X(96)00022-4.
[16] Perren RA, et al. Corrosion resistance of super duplex stainless steels in chloride ion containing environments: investigations by means of a new microelectrochemical method I. Precipitation-free states. Corros Sci 2001;43:707–26 https://doi.org/10.1016/S0010-938X(00)00087-1.
[17] Saeid T, Abdollah-Zadeh A, Assadi H, Ghaini FM. Effect of friction stir welding speed on the microstructure and mechanical properties of duplex stainless steel. Mater Sci Eng A 2008;496:262–8 https://doi.org/10.1016/j.msea.2008.05.025.
[18] Santos TFA, Lopez EAT, Fonseca EB, Ramirez AJ. Friction stir welding of the duplex and super duplex stainless steels and some aspects of microstructural characterization and mechanical performance. Mater Res 2016;19:117–31 https://doi.org/10.1590/1980-5373-MR-2015-0319.
[19] Magnani M, et al. Microstructural and electrochemical characterization of friction stir welded duplex stainless steels. Int J Electrochem Sci 2014;9:2966–77.
[20] Sarlak H, Atapour M, Esmailzadeh M. Corrosion behaviour of friction stir welded lean duplex stainless steel. Mater Des 2015;66:209–16 https://doi.org/10.1016/j.matdes.2014.10.060.
[21] Park SHC, Sato YS, Kokawa H, Okamoto K, Hirano S, Inagaki M. Rapid formation of the sigma phase in 304 stainless steel during friction stir welding. Scr Mater 2004;51:101.
[22] Garcia C, Martin F, de Tiedra P, Blanco Y, Lopez M. Pitting corrosion of welded joints of austenitic stainless steels studied by using an electrochemical minicell. Corros Sci 2008;50:1184.
[23] Zhang Z, Zhang H, Zhao H, Li J. Effect of prolonged thermal cycles on the pitting corrosion resistance of a newly developed LDX 2404 lean duplex stainless steel. Corros Sci 2016;103:189–95 https://doi.org/10.1016/j.corsci.2015.11.018.
[24] Canderyd C, Pettersson R, Johansson M. Properties of the new duplex grade LDX 2404®. In: Stainless steel world conference & expo 2011. 2011. p. 13 p.
[25] Zhao H, Zhang Z, Zhang H, Hu J, Li J. Effect of aging time on intergranular corrosion behaviour of a newly developed LDX

2404 lean duplex stainless steel. J Alloys Compd 2016;672:147–54 https://doi.org/10.1016/j.jallcom.2016.02.101.
[26] Outukumpu Grade Data Sheet LDX 2402.
[27] "Standard test methods for detecting detrimental intermetallic phase in duplex austenitic/ferritic stainless steels," ASTM A923-14, in Annual Book of ASTM Standards, vol. 01.03.
[28] "Standard guide for quantitative analysis by energy-dispersive spectroscopy," ASTM E1508-12, in Annual Book of ASTM Standards, vol. 03.01.
[29] Garfias-Mesias LF. Understanding why PREN alone cannot be used to select duplex stainless steels. In: Corrosion 2015 conference & expo. 2015.
[30] Wolynec S. Electrochemical techniques in corrosion. first ed. São Paulo: EDUSP; 2003.
[31] "Standard test method for electrochemical critical pitting temperature testing of stainless steels," ASTM G150-13, in Annual Book of ASTM Standards, vol. 03.02.
[32] Arnvig P-E, Bisgard AD. Determining the potential independent critical pitting temperature (CPT) by a potentiostatic method using the Avesta cell. In: Corrosion 1996 conference & expo. 1996.
[33] Santos TFA, Torres EA, Ramirez AJ. Friction stir welding of duplex stainless steels. Welding Int 2017;32:1–9 https://doi.org/10.1080/09507116.2017.1347323.
[34] Canderyd C, Pettersson R. UNS S82441 – a new duplex stainless steel grade for the process industries. In: Corrosion 2012 conference & expo. 2012.
[35] Forgas A Jr, Marangoni J, Otubo J, Donato GHB, Magnabosco R. Reverse strain-induced martensitic transformation of the ferrite to austenite in duplex stainless steels. J Mater Sci 2016;51:10452–63 https://link.springer.com/article/10.1007/s10853-016-0265-1.
[36] Heyn A, Goellner J, Burkert A. Determination of critical pitting temperatures using electrochemical noise. In: Corrosion 2004 conference & expo. 2004.
[37] Dong C, Luo H, Xiao K, Sun T, Liu Q, Li X. Effect of temperature and Cl-concentration on pitting of 2205 duplex stainless steel. J Wuhan Univ Technol Mat Sci Ed 2011;26:641–7 https://doi.org/10.1007/s11595-011-0283-4.
[38] Deng B, Jiang Y, Gong J, Zhong C, Gao J, Li J. Critical pitting and repassivation temperatures for duplex stainless steel in chloride solutions. Electrochim Acta 2008;53:5220–5 https://doi.org/10.1016/j.electacta.2008.02.047.
[39] Ebrahimi N, Moayed MH, Davoodi A. Critical pitting temperature dependence of 2205 duplex stainless steel on dichromate ion concentration in chloride medium. Corros Sci 2011;53:1278–87 https://doi.org/10.1016/j.corsci.2010.12.019.
[40] Eghbali F, Moayed MH, Davoodi A, Ebrahimi N. Critical pitting temperature (CPT) assessment of 2205 duplex stainless steel in 0.1 M NaCl at various molybdate concentrations. Corros Sci 2011;53:513–22 https://doi.org/10.1016/j.corsci.2010.08.008.
[41] Sicupira DC, Frankel GS, Lin VFC. Pitting corrosion of welds in UNS S32304 lean duplex stainless steel. Mater Corr 2015;67:440–8 https://doi.org/10.1002/maco.201508502.
[42] Miura M, Koso M, Kudo T, Tsuge H. Effect of nickel and nitrogen on microstructure and corrosion resistance of duplex stainless steel weldment. Q J Jpn Weld Soc 1989;7:94–100 https://doi.org/10.2207/qjjws.7.94.
[43] Lothongkum G, Wongpanya P, Morito S, Furuhara T, Maki T. Effect of nitrogen on corrosion behavior of the 28Cr–7Ni duplex and micro duplex stainless steels in air-saturated 3.5 wt% NaCl solution. Corros Sci 2006;48:137–53 https://doi.org/10.1016/j.corsci.2004.11.017.